Progress In Electromagnetics Research B, Vol. 21, 27–45, 2010

ESTIMATION OF ERROR INDUCED BY A CROSSED-DIPOLE PROBE IN THE NEAR-FIELD

S. Paramesha

Department of E & C
AIT, Chikmagalur, Karnataka 577102, India

A. Chakrabarty

Department of E & ECE
IIT, Kharagpur, West Bengal 721302, India

Abstract—The Moment Method is used to estimate the error induced by a compact measuring probe in the near-field. A crossed-dipole is used as a compact near-field measuring probe of a waveguide radiator in an infinite ground plane, since it measures both co-pole and cross-pole components simultaneously. However, due to multiple reflections between radiator and probe, in addition, mutual coupling effects between the poles, near-field values are changed. The relative sampled electric field pattern (without the probe) is compared to the relative sampled co-pole voltage pattern in the scan plane and the induced error is computed. The radiating waveguide's reflection coefficient is altered with respect to the reflection coefficient when there is no probe in the near-field. The numerical results concerning the reflection coefficient without the probe are compared to the measured values, and good agreement is observed.

1. INTRODUCTION

If the test antenna is reciprocal, the receiving mode characteristics (gain, radiation pattern etc.) are identical to those transmitted by the antenna. The ideal condition for measuring far-field radiation characteristics then, is the illumination of the test antenna by a plane waves: uniform amplitude and phase. Although this ideal condition is not achievable, it can be approximated by separating the test antenna from the illumination source by a large distance on an outdoor range.

Corresponding author: S. Paramesha (prm_ait@yahoo.com).

At large radii, the curvature of the spherical phasefront produced by the source antenna is small over the test antenna aperture. If the separation distance is equal to the inner boundary of the far-field region, $2D^2/\lambda$ then the maximum phase error of the incident field from an ideal plane wave is about 22.5 degrees. In addition to phasefront, curvature due to finite separation distances, reflections from ground and nearby objects are possible sources of degradation of the test antenna illumination.

Experimental investigations suffer from a number of drawbacks such as: 1) For pattern measurements, the distance to the far-field region is too long even for outside ranges. It also becomes difficult to keep unwanted reflections from the ground and the surrounding objects below acceptable level. 2) In many cases, it may be impractical to move the antenna from the operating environment to the measuring site. 3) For some antennas, such as phased arrays, the time required to measure the necessary characteristics may be enormous. 4) Outside measuring systems provide an uncontrolled environment, and they do not posses an all-weather capability. 5) Enclosed measuring systems usually cannot accommodate large antenna systems (such as ships, aircrafts, large spacecrafts, etc.). 6) Measurement technique, in general, are expensive. Some of the shortcomings can be overcome by using special techniques, such as indoor measurements, far-field pattern prediction from near-field measurements, etc.

The radiating structure used in the analysis is the open end of a waveguide, terminated by an infinite metallic flange. The Method of Moments is used to solve many waveguide and wire antenna problems [1–3]. The application of the Moment Method using the entire domain basis function [4] converts the integral equations representing the boundary condition at waveguide aperture into matrix equations, from which, the coefficients of the basis functions representing the aperture field can be evaluated.

The crossed-dipole being used as a near-field measuring probe consists of two dipoles oriented orthogonal to each other, and the cross-dipole is sensitive to electric field components oriented parallel to the axis of the co-pole and cross-pole of the probe. The scattering properties of the objects are polarization dependent. The ability of the receive antenna to measure these scattered fields is determined by the polarization match between the scattered fields and the polarization of the receive antenna. A complex polarization mismatch using dipole antennas results when the scattered field and the polarization of the receive antenna are both linearly polarized and oriented at right angles to each other. Using a crossed-dipole probe, both co-pole and cross-pole near-field components can be sampled simultaneously in the scan

plane; however, the probe itself induces error because of multiple reflections and mutual coupling effect [5].

2. FORMULATION OF THE PROBLEM

The crossed-dipole in the near-field of an open-ended waveguide radiator of aperture dimension $2a \times 2b$ in an infinite ground plane is shown in Figure 1. The waveguide feeding the rectangular aperture is assumed to be excited in the dominant TE_{10} mode.

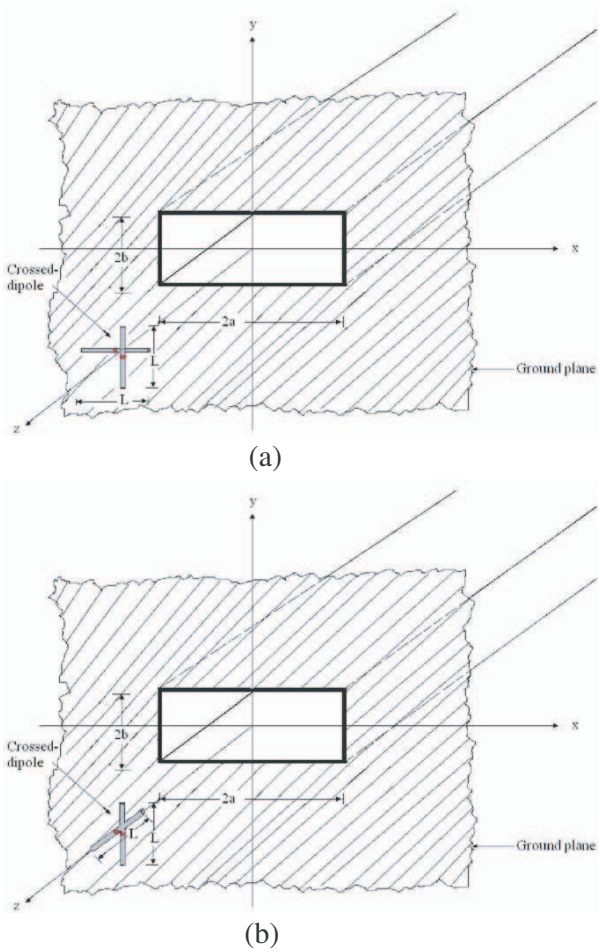

Figure 1. Crossed-dipole probe at the near-field of the waveguide radiator. (a) Probe in x-y plane. (b) Probe in y-z plane.

The incident magnetic field at the waveguide aperture for the dominant TE_{10} mode is given by:

$$H_x^{inc} = -Y_0 \cos\left(\frac{\pi x}{2a}\right) e^{-j\beta z} \tag{1}$$

and the electric field at the radiating aperture is described by:

$$\overrightarrow{E}(x', y', 0) = \hat{u}_y \sum\nolimits_{p=1}^{M} E_p e_p \tag{2}$$

where the entire domain basis functions $e_p, (p = 1, 2, \ldots, M)$ are defined by:

$$e_p = \begin{cases} \sin\left\{\frac{p\pi}{2a}(x+a)\right\} & \begin{cases} -a \le x \le a \\ -b \le y \le b \end{cases} \\ 0 & \text{elsewhere} \end{cases} \tag{3}$$

The equivalent magnetic current at the waveguide aperture for computing the externally scattered field obtained as:

$$\begin{aligned} \vec{M}_e &= 2\vec{E}(x', y', 0) \times \hat{u}_z \\ &= \hat{u}_x \sum\nolimits_{p=1}^{M} 2E_p \sin\left\{\frac{p\pi}{2a}(x+a)\right\} \begin{cases} -a \le x \le a \\ -b \le y \le b \end{cases} \end{aligned} \tag{4}$$

The radius of the co-pole and cross-pole of the crossed-dipole probe are assumed to be much smaller than the length L and wavelength λ. With good accuracy, the surface current density on the thin conducting wire can be considered to have only an axial component [3].

The induced current on the surface of the co-pole (parallel to y-axis) of the near-field probe is described by:

$$I = \hat{u}_y \sum\nolimits_{p=1}^{M} I_{yp} i_{yp} \tag{5}$$

where the Pulse basis function i_{yp} $(p = 1, 2, 3, \ldots, M)$ are defined by

$$i_{yp} = \begin{cases} 1 & y'_{p-1} \le y' \le y'_p \\ 0 & \text{elsewhere} \end{cases} \tag{6}$$

I_{yp} are the coefficients of the pulse basis function for the co-pole.

Similarly, we can describe induced current I_x (I_z) on the surface of the cross-pole, when it is parallel to x (z) axis.

The radiated magnetic field at the plane of the waveguide aperture is evaluated using the plane-wave spectrum approach and it is given

by:

$$H_x^{ext} = -\frac{ab}{\pi^2 k\eta}\sum_{p=1}^{M} E_p \int_{-\infty}^{\infty}\int_{-\infty}^{\infty} \frac{k^2-k_x^2}{\left(k^2-k_x^2-k_y^2\right)^{1/2}}\mathrm{sinc}(k_y b) \frac{\left\{\begin{array}{l} j\sin(k_x a)\ p \text{ even} \\ \cos(k_x a)\ p \text{ odd}\end{array}\right\}}{\frac{p\pi}{2}\left\{1-\left(\frac{2ak_x}{p\pi}\right)^2\right\}} e^{j(k_x x+k_y y)}dk_x dk_y \quad (7)$$

The radiated electric field at the near-field probe is also evaluated using the plane-wave spectrum approach and described below:

$$E_x = 0 \quad (\text{since } \varepsilon_x = 0) \quad (8)$$

$$E_y = \frac{1}{2\pi}\int_{-\infty}^{\infty}\int_{-\infty}^{\infty} \varepsilon_y e^{j(k_x x+k_y y-k_z z)}dk_x dk_y \quad (9)$$

$$E_z = -\frac{1}{2\pi}\int_{-\infty}^{\infty}\int_{-\infty}^{\infty} \frac{\varepsilon_y k_y}{k_z} e^{j(k_x x+k_y y-k_z z)}dk_x dk_y \quad (10)$$

ε_y is the Fourier Transform of the electric field at the radiating aperture and is given by

$$\varepsilon_y(k_x,k_y,k) = \frac{1}{2\pi}\sum_{p=1}^{M} E_p \iint \sin\left\{\frac{p\pi}{2a}(x'+a)\right\} e^{-j\left(k_x x'+k_y y'\right)}dx'dy'$$

After substituting and simplifying, we obtained:

$$E_y = \frac{ab}{\pi^2}\sum_{p=1}^{M} E_p \int_{-\infty}^{\infty}\int_{-\infty}^{\infty} \mathrm{sinc}(k_y b)\frac{\left\{\begin{array}{l} j\sin(k_x a)\ p \text{ even} \\ \cos(k_x a)\ p \text{ odd}\end{array}\right\}}{\frac{p\pi}{2}\left\{1-\left(\frac{2ak_x}{p\pi}\right)^2\right\}} e^{j(k_x x_1+k_y y_1-k_z z_1)}dk_x dk_y \quad (11)$$

$$E_z = -\frac{ab}{\pi^2}\sum_{p=1}^{M} E_p \int_{-\infty}^{\infty}\int_{-\infty}^{\infty} \frac{k_y}{k_z}\mathrm{sinc}(k_y b)\frac{\left\{\begin{array}{l} j\sin(k_x a)\ p \text{ even} \\ \cos(k_x a)\ p \text{ odd}\end{array}\right\}}{\frac{p\pi}{2}\left\{1-\left(\frac{2ak_x}{p\pi}\right)^2\right\}} e^{j(k_x x_1+k_y y_1-k_z z_1)}dk_x dk_y \quad (12)$$

We obtained the internally scattered magnetic field by using the

modal expansion approach; the x-component of the field is given by:

$$H_x^{int} = \sum_{p=1}^{M} E_p Y_{p0}^e \sin\left\{\frac{m\pi}{2a}(x+a)\right\} \tag{13}$$

At any observation point, the y-component of the electric field scattered by the induced current on the co-pole is given by:

$$E_y^s = \frac{\lambda\sqrt{\mu/\in}}{16\pi^3 j} \int_{y'=-L/2}^{L/2} \int_{\phi'=0}^{2\pi} I_{yp} \frac{e^{-jkR_1}}{R_1^5} \left[(1+jkR_1)\left(2R_1^2 - 3a_w^2\right) + k^2 a_w^2 R_1^2\right] dy' d\phi' \tag{14}$$

where

$$R_1 = \sqrt{\rho^2 + a_w^2 - 2\rho a_w \cos\phi' + (y-y')^2} \tag{15}$$

and a_w is the radius of the pole, ρ is the radial distance to the observation point.

For observation on the axis of the co-pole ($\rho = 0$),

$$R_1 = \sqrt{a_w^2 + (y-y')^2} \tag{16}$$

and

$$E_y^s = \frac{\lambda\sqrt{\mu/\in}}{8\pi^2 j} \int_{-L/2}^{L/2} I_{yp} \frac{e^{-jkR_1}}{R_1^5} \left[(1+jkR_1)\left(2R_1^2 - 3a_w^2\right) + k^2 a_w^2 R_1^2\right] dy' \tag{17}$$

Similarly, the field on the axis of the cross-pole (oriented along x-axis) scattered by the induced current on that pole is given by:

$$E_x^s = \frac{\lambda\sqrt{\mu/\in}}{8\pi^2 j} \int_{-L/2}^{L/2} I_{xp} \frac{e^{-jkR_2}}{R_2^5} \left[(1+jkR_2)\left(2R_2^2 - 3a_w^2\right) + k^2 a_w^2 R_2^2\right] dx' \tag{18}$$

where

$$R_2 = \sqrt{a_w^2 + (x-x')^2} \tag{19}$$

If the probe is in y-z plane and cross-pole axis is parallel to the z-axis, then electric field on the axis of the cross-pole scattered by the induced current on that pole is given by:

$$E_z^s = \frac{\lambda\sqrt{\mu/\in}}{8\pi^2 j} \int_{-L/2}^{L/2} I_{zp} \frac{e^{-jkR_3}}{R_3^5} \left[(1+jkR_3)\left(2R_3^2 - 3a_w^2\right) + k^2 a_w^2 R_3^2\right] dz' \tag{20}$$

where

$$R_3 = \sqrt{a_w^2 + (z - z')^2} \tag{21}$$

The electric field on the axis of the co-pole due to current on the cross-pole (mutual coupling effect) is obtained as:

$$E_y^{mx} = \frac{\lambda\sqrt{\mu/\varepsilon}}{16\pi^3 j} \int_{x'=-L/2}^{L/2} \int_{\phi'=0}^{2\pi} I_{xp} \frac{e^{-jkR_4}(x-x')(y-y')(3+3jkR_4-k^2R_4^2)}{R_4^5} dx'd\phi' \tag{22}$$

where $R_4 = \sqrt{\rho^2 + a_w^2 - 2\rho a_w \cos\phi' + (x - x')^2}$ and the field on the cross-pole due to current on the co-pole is given by:

$$E_x^{my} = \frac{\lambda\sqrt{\mu/\varepsilon}}{16\pi^3 j} \int_{y'=-L/2}^{L/2} \int_{\phi'=0}^{2\pi} I_{yp} \frac{e^{-jkR_5}(x-x')(y-y')(3+3jkR_5-k^2R_5^2)}{R_5^5} dy'd\phi' \tag{23}$$

The expression for R_5 is same as (15).

The x-component of the magnetic field at the plane of the waveguide aperture scattered by the induced current on the co-pole of the probe is obtained as:

$$H_x^s = \int_{y'=-L/2}^{L/2} \int_{\phi'=0}^{2\pi} I_{yp} \frac{e^{-jkR_6}}{8\pi^2 R_6^3} (\rho - a_w \cos\phi') \{1 + jkR_6\} dy'd\phi' \tag{24}$$

The expression for R_6 is same as (15).

3. IMPOSITION OF BOUNDARY CONDITION

The boundary conditions are imposed at the plane of the waveguide aperture, on the axis of the co-pole and on the axis of the cross-pole. The boundary condition at the region of the waveguide aperture is the tangential component of the magnetic field both inside and outside the waveguide is identical. The boundary condition on the axis of the pole is the total tangential component of the electric field is zero.

At the region of the aperture, we consider four sources producing the fields — (i) The source in the waveguide exciting the TE_{10} mode, (ii) the magnetic current source at the aperture, (iii) the electric current source on the surface of the co-pole, and (iv) the electric current source on the surface of the cross-pole. Using the principle of superposition,

the x-component of the magnetic field at the plane of the aperture is derived. In the analysis, two cases have been considered: **First case** (the co-pole axis is parallel to the y-direction and the cross-pole axis is parallel to the x-direction); **Second case** (the co-pole axis is parallel to the y-direction and the cross-pole axis is parallel to the z-direction).

First case: At the plane of the waveguide aperture (at the $z = 0$ plane), using superposition:

$$H_x^{int/1} + H_x^{int/2} + H_x^{int/3} + H_x^{int/4} = H_x^{ext/1} + H_x^{ext/2} + H_x^{ext/3} + H_x^{ext/4}$$

or,

$$2H_x^{inc} + H_x^{int1} = H_x^{ext1} + H_x^{extco1} + H_x^{extcr1} \tag{25}$$

Along the axis of the co-pole and cross-pole, the fields are respectively given by

$$E_y^{inc1} + E_y^{mx1} + E_y^{scat1} = 0 \tag{26}$$

$$E_x^{inc1} + E_x^{my1} + E_x^{scat1} = 0 \tag{27}$$

The superscript 1 indicates First case. H_x^{extco} is the x-component of the magnetic field at the aperture scattered by the induced current on the co-pole; H_x^{extcr} is the x-component of the magnetic field at the aperture scattered by the induced current on the cross-pole. E_y^{inc} is the incident electric field at the co-pole, radiated by the waveguide, E_y^{mx} is the field in the co-pole due to induced current on the cross-pole (mutual coupling effect) and E_y^{scat} is the y-component of the scattered field due to the induced current on the co-pole. Similarly, E_x^{inc} is the incident electric field at the cross-pole, E_x^{my} is the field in the cross-pole due to induced current on the co-pole (mutual coupling effect) and E_x^{scat} is the x-component of the scattered field due to induced current on the cross-pole.

Second case: At the plane of the waveguide aperture (at the $z = 0$ plane), using superposition:

$$H_x^{int1} + H_x^{int/2} + H_x^{int/3} + H_x^{int/4} = H_x^{ext/1} + H_x^{ext/2} + H_x^{ext/3 + H_x^{ext/4}}$$

or,

$$2H_x^{inc} + H_x^{int2} = H_x^{ext2} + H_x^{extco2} + H_x^{extcr2} \tag{28}$$

Along the axis of the co-pole and cross-pole, the fields are respectively given by

$$E_y^{inc2} + E_y^{mz2} + E_y^{scat2} = 0 \tag{29}$$

$$E_z^{inc2} + E_z^{my2} + E_z^{scat2} = 0 \tag{30}$$

The superscript 2 indicates Second case.

4. SOLVING FOR THE APERTURE ELECTRIC FIELD AND PROBE CURRENTS

To determine the electric field and current distributions at the waveguide aperture and on the probe respectively, it is necessary to determine the basis function coefficients.

Since the field at the aperture is described by M basis functions, M unknowns are to be determined from the boundary condition. The weighting functions and the moment of the field are defined as below [6]:

$$w_q^1 = \begin{cases} \sin\left\{\frac{q\pi}{2a}(x+a)\right\} & \begin{cases} -a \le x \le a \\ -b \le y \le b \end{cases} \\ 0 & \text{elsewhere} \end{cases} \tag{31}$$

$$\left\langle H, w_q^1 \right\rangle = \iint\limits_{Aperture} H \cdot w_q^1 dxdy \tag{32}$$

In addition, since the current on the pole of the probe is described by M basis functions, M unknowns are to be determined from the boundary condition. The weighting functions and the moment of the field are defined as:

$$w_q^2 = [\delta(h - h_q)] = [\delta(h - h_1), \delta(h - h_2), \ldots] \tag{33}$$

where h specifies a position with respect to some reference (origin), and h_q represents a point at which the boundary condition is enforced.

$$\left\langle E, w_q^2 \right\rangle = \iint\limits_{surface} E \cdot w_q^2 ds \tag{34}$$

w_q^1 and w_q^2 are the entire domain and point matching weighting (testing) functions at the waveguide aperture and pole axis respectively.

For the **First case**, using the boundary conditions given by (25), (26) and (27), and the definition in (32) and (34), and converting into matrix form:

$$2\left[L^{inc}\right]+\left[L^{int1}\right]\left[E_p^1\right]=\left[L^{ext1}\right]\left[E_p^1\right]+\left[L^{extco1}\right]\left[I_{yp}^1\right]+\left[L^{extcr1}\right]\left[I_{xp}^1\right] \tag{35}$$

$$\left[L^{coinc1}\right]\left[E_p^1\right] + \left[L^{ymx1}\right]\left[I_{xp}^1\right] + \left[L^{coscat1}\right]\left[I_{yp}^1\right] = 0 \tag{36}$$

$$\left[L^{crinc1}\right]\left[E_p^1\right] + \left[L^{xmy1}\right]\left[I_{yp}^1\right] + \left[L^{crscat1}\right]\left[I_{xp}^1\right] = 0 \tag{37}$$

For the **Second case**, using the boundary conditions given by (28), (29) and (30), and the definition in (32) and (34), and

converting into matrix form:

$$2\left[L^{inc}\right]+\left[L^{int2}\right]\left[E_p^2\right]=\left[L^{ext2}\right]\left[E_p^2\right]+\left[L^{extco2}\right]\left[I_{yp}^2\right]+\left[L^{extcr2}\right]\left[I_{zp}^2\right] \quad (38)$$

$$\left[L^{coinc2}\right]\left[E_p^2\right]+\left[L^{ymz2}\right]\left[I_{zp}^2\right]+\left[L^{coscat2}\right]\left[I_{yp}^2\right]=0 \quad (39)$$

$$\left[L^{crinc2}\right]\left[E_p^2\right]+\left[L^{zmy2}\right]\left[I_{yp}^2\right]+\left[L^{crscat2}\right]\left[I_{zp}^2\right]=0 \quad (40)$$

The moments of the incident and scattered fields are given by:

$$\begin{aligned}\left[L^{inc}\right]&=L_q^{inc}=\left\langle H_x^{inc},w_q^1\right\rangle\\&=-Y_0\int_{-a}^{a}\int_{-b}^{b}\cos\left(\frac{\pi x}{2a}\right)\sin\left\{\frac{q\pi}{2a}\left(x+a\right)\right\}dxdy\\&=\begin{cases}-2abY_0 & q=1\\0 & \text{otherwise}\end{cases}\end{aligned} \quad (41)$$

$$\begin{aligned}\left[L^{int1}\right]&=L_{q,p}^{int1}=\left\langle H_x^{int1}\left(e_p\right),w_q^1\right\rangle\\&=Y_{p0}^e\int_{-a}^{a}\int_{-b}^{b}\sin\left\{\frac{q\pi}{2a}\left(x+a\right)\right\}\sin\left\{\frac{m\pi}{2a}(x+a)\right\}dxdy\\&=\begin{cases}2abY_{p0}^e & p=q=m,\ n=0\\0 & \text{otherwise}\end{cases}\end{aligned} \quad (42)$$

$$\begin{aligned}\left[L^{ext1}\right]&=L_{q,p}^{ext1}=\left\langle H_x^{ext1}\left(e_p\right),w_q^1\right\rangle\\&=-\frac{ab}{\pi^2k\eta}\int_{-\infty}^{\infty}\int_{-\infty}^{\infty}\frac{k^2-k_x^2}{\left(k^2-k_x^2-k_y^2\right)^{1/2}}\operatorname{sinc}(k_yb)\frac{\begin{Bmatrix}j\sin\left(k_xa\right)\ \text{p even}\\\cos\left(k_xa\right)\ \text{p odd}\end{Bmatrix}}{\frac{p\pi}{2}\left\{1-\left(\frac{2ak_x}{p\pi}\right)^2\right\}}\\&\quad\int_{-a}^{a}\int_{-b}^{b}\sin\left\{\frac{q\pi}{2a}\left(x+a\right)\right\}e^{j(k_xx+k_yy)}dxdydk_xdk_y\\&=-\frac{4a^2b^2}{\pi^2k\eta}\int_{-\infty}^{\infty}\int_{-\infty}^{\infty}\frac{\left(k^2-k_x^2\right)}{\left(k^2-k_x^2-k_y^2\right)^{1/2}}\operatorname{sinc}^2\left(k_yb\right)\\&\quad\frac{\begin{Bmatrix}\sin^2\left(k_xa\right) & p,\ q\ \text{both even}\\\cos^2\left(k_xa\right) & p,\ q\ \text{both odd}\\0 & \text{otherwise}\end{Bmatrix}}{\frac{p\pi}{2}\left\{1-\left(\frac{2ak_x}{p\pi}\right)^2\right\}\frac{q\pi}{2}\left\{1-\left(\frac{2ak_x}{q\pi}\right)^2\right\}}dk_xdk_y\end{aligned} \quad (43)$$

To carry out the integral in the spectral domain, we make the

following substitutions to obtain the real and imaginary parts of the integral:

$$\begin{aligned} k_x &= k\sin\theta\cos\phi \\ k_y &= k\sin\theta\sin\phi \\ dk_x dk_y &= k^2\sin\theta\cos\theta d\theta d\phi \end{aligned} \tag{44}$$

in the visible region, i.e., $k_x^2 + k_y^2 \leq k^2$, and

$$\begin{aligned} k_x &= k\cosh\theta\cos\phi \\ k_y &= k\cosh\theta\sin\phi \\ dk_x dk_y &= k^2\sinh\theta\cosh\theta d\theta d\phi \end{aligned} \tag{45}$$

in the invisible region, where $k_x^2 + k_y^2 \succ k^2$. The final expressions for the elements of the moment matrices are obtained as:

$$\begin{aligned} &L_{q,p\ \text{visible region}}^{ext1} \\ &= -\frac{16a^2b^2}{\lambda^2\eta}\int_{\theta=0}^{\frac{\pi}{2}}\int_{\phi=0}^{2\pi}\left(1-\sin^2\theta\cos^2\varphi\right)\text{sinc}^2\left(bk\sin\theta\sin\phi\right) \\ &\quad \frac{\left\{\begin{array}{ll}\sin^2\left(ak\sin\theta\cos\phi\right) & p,\ q \text{ both even} \\ \cos^2\left(ak\sin\theta\cos\phi\right) & p,\ q \text{ both odd} \\ 0 & \text{otherwise}\end{array}\right\}}{\frac{p\pi}{2}\left\{1-\left(\frac{2ak\sin\theta\cos\phi}{p\pi}\right)^2\right\}\frac{q\pi}{2}\left\{1-\left(\frac{2ak\sin\theta\cos\phi}{q\pi}\right)^2\right\}}\sin\theta d\theta d\phi \end{aligned} \tag{46}$$

$$\begin{aligned} &L_{q,p\ \text{invisible region}}^{ext1} \\ &= -j\frac{16a^2b^2}{\lambda^2\eta}\int_{\theta=0}^{\infty}\int_{\phi=0}^{2\pi}\left(1-\cosh^2\theta\cos^2\phi\right)\text{sinc}^2\left(bk\cosh\theta\sin\phi\right) \\ &\quad \frac{\left\{\begin{array}{ll}\sin^2\left(ak\cosh\theta\cos\phi\right) & p,\ q \text{ both even} \\ \cos^2\left(ak\cosh\theta\cos\phi\right) & p,\ q \text{ both odd} \\ 0 & \text{otherwise}\end{array}\right\}}{\frac{p\pi}{2}\left\{1-\left(\frac{2ak\cosh\theta\cos\phi}{p\pi}\right)^2\right\}\frac{q\pi}{2}\left\{1-\left(\frac{2ak\cosh\theta\cos\phi}{q\pi}\right)^2\right\}}\cosh\theta d\theta d\phi \end{aligned} \tag{47}$$

$$\begin{aligned} &\left[L^{extco1}\right] = L_{q,p}^{extco1} = \left\langle H_x^{extco1}\left(i_{yp}\right), w_q^1\right\rangle \\ &= \int_{y'=-L/2}^{L/2}\int_{\phi'=0}^{2\pi}\frac{e^{-jkR}}{8\pi^2R_6^3}\left(\rho-a_w\cos\phi'\right)\left(1+jkR_6\right)\left\{\begin{array}{ll}0 & q \text{ even} \\ \frac{8ab}{q\pi} & q \text{ odd}\end{array}\right\}dy'd\phi' \end{aligned} \tag{48}$$

$$\left[L^{extcr1}\right] = L_{q,p}^{extcr1} = \left\langle H_x^{extcr1}\left(i_{xp}\right), w_q^1\right\rangle = 0 \tag{49}$$

$$\left[L^{coinc1}\right] = L^{coinc1}_{q,p} = \left\langle E^{inc1}_{y}\left(e_p\right), w^2_q\right\rangle$$

$$= \frac{ab}{\pi^2}\int\limits_{-\infty}^{\infty}\int\limits_{-\infty}^{\infty}\mathrm{sinc}(k_y b)\frac{\begin{Bmatrix} j\sin\left(k_x a\right) & p \text{ even} \\ \cos(k_x a) & p \text{ odd}\end{Bmatrix}}{\frac{p}{2}\left\{1-\left(\frac{2ak_x}{p\pi}\right)^2\right\}} e^{-j(k_x x_1 + k_y y + k_z z)}dk_x dk_y \quad (50)$$

$$\left[L^{ymx1}\right] = \left\langle E^{mx1}_{y}\left(i_{xp}\right), w^2_q\right\rangle = \frac{\lambda\sqrt{\mu/\varepsilon}}{16\pi^3 j}$$

$$\int\limits_{x'=-L/2}^{L/2}\int\limits_{\phi'=0}^{2\pi} e^{-jkR_4}\frac{(x-x')(y-y')(3+3jkR_4-k^2R_4^2)}{R_4^5}dx'd\phi' \quad (51)$$

$$\left[L^{\cos cat1}\right] = L^{coscat1}_{q,p} = \left\langle E^{scat1}_{y}\left(i_{yp}\right), w^2_q\right\rangle$$

$$= \frac{\lambda\sqrt{\mu/\varepsilon}}{8\pi^2 j}\int\limits_{-L/2}^{L/2}\frac{e^{-jkR_1}}{R_1^5}\left[\left(1+jkR_1\right)\left(2R_1^2-3a_w^2\right)+k^2a_w^2R_1^2\right]dy' \quad (52)$$

$$\left[L^{crinc1}\right] = L^{crinc1}_{q,p} = \left\langle E^{inc1}_{x}\left(e_p\right), w^2_q\right\rangle = 0 \quad (53)$$

$$\left[L^{xmy1}\right] = L^{xmy1}_{q,p} = \left\langle E^{my1}_{x}\left(i_{yp}\right), w^2_q\right\rangle$$

$$= \frac{\lambda\sqrt{\mu/\varepsilon}}{16\pi^3 j}\int\limits_{-L/2}^{L/2}\int\limits_{\phi'=0}^{2\pi} e^{-jkR_5}\frac{(x-x')(y-y')(3+3jkR_5-k^2R_5^2)}{R_5^5}dy'd\phi' \quad (54)$$

$$\left[L^{crscat1}\right] = L^{crscat1}_{q,p} = \left\langle E^{scat1}_{x}\left(i_{xp}\right), w^2_q\right\rangle$$

$$= \frac{\lambda\sqrt{\mu/\varepsilon}}{8\pi^2 j}\int\limits_{-L/2}^{L/2}\frac{e^{-jkR_2}}{R_2^5}\left[\left(1+jkR_2\right)\left(2R_2^2-3a_w^2\right)+k^2a_w^2R_2^2\right]dx' \quad (55)$$

From Equations (35), (36) and (37), solving coefficients E^1_p, I^1_{yp} and I^1_{xp} we obtain:

$$\begin{bmatrix}\left[E^1_p\right]\\ \left[I^1_{yp}\right]\\ \left[I^1_{xp}\right]\end{bmatrix} = \begin{bmatrix}\left[L^{ext1}\right]-\left[L^{int1}\right] & \left[L^{extco1}\right] & \left[L^{extcr1}\right]\\ \left[L^{coinc1}\right] & \left[L^{coscat1}\right] & \left[L^{ymx1}\right]\\ \left[L^{crinc1}\right] & \left[L^{xmy1}\right] & \left[L^{crscat1}\right]\end{bmatrix}^{-1}\begin{bmatrix}2\left[L^{inc}\right]\\ [0]\\ [0]\end{bmatrix} \quad (56)$$

If M basis functions are used to describe the electric field at the radiating aperture then there are M unknowns, namely, E_p $(p = 1, 2, \ldots, M)$ and to solve for these, M weighting functions w^1_q $(q = 1, 2, \ldots, M)$ are required. Similarly, if M basis functions

are used to describe the current on the surface of the pole of the probe, namely, I_p $(p = 1, 2, \ldots, M)$ and to solve for these, M weighting functions w_q^2 $(q = 1, 2, \ldots, M)$ are required.

Reflection coefficient Γ^1 (in the First case) is given by:

$$\Gamma^1 = -1 + E_1^1 \tag{57}$$

The pole voltage of the probe is then obtained across 50 ohms terminating impedance [7].

Similarly, from Equations (38), (39) and (40), the coefficients E_p^2, I_{yp}^2 and I_{zp}^2 can be obtained for the Second case:

$$\begin{bmatrix} [E_p^2] \\ [I_{yp}^2] \\ [I_{xp}^2] \end{bmatrix} = \begin{bmatrix} [L^{ext2}] - [L^{int2}] & [L^{extco2}] & [L^{extcr2}] \\ [L^{coinc2}] & [L^{coscat2}] & [L^{ymx2}] \\ [L^{crinc2}] & [L^{xmy2}] & [L^{crscat2}] \end{bmatrix}^{-1} \begin{bmatrix} 2[L^{inc}] \\ [0] \\ [0] \end{bmatrix} \tag{58}$$

5. RESULTS AND DISCUSSION

The aperture in an infinite ground plane fed by a standard X-band WR-90 rectangular waveguide is used as a radiator, and two dipoles, each of length 0.47λ and radius 0.005λ, in crossed configuration are used as a near-field probe. The lumped load of $50\,\Omega$ is connected at the centre of each pole and the junction of the cross is at a distance of one segment (one pulse basis function) away from the center of

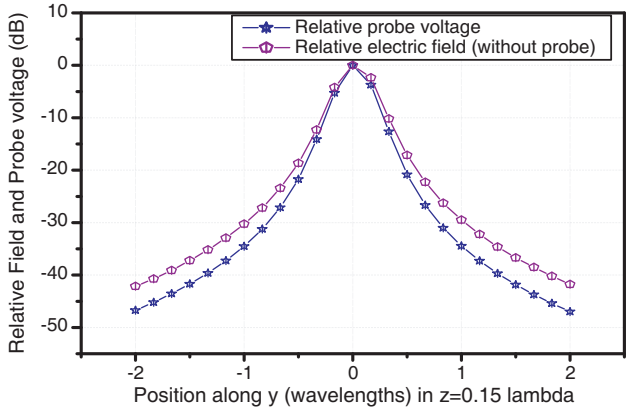

Figure 2. Relative sampled electric field (without probe) and relative sampled co-pole voltage in x-y plane at $x = 0$, $z = 0.15\lambda$, and at 10 GHz.

the poles as shown in Figure 1. The junction (cross) point of the probe is taken as the reference point in the computation. For the determination of the coefficients of the basis functions, the program written in MATLAB 7 was run on a 3 GHz Pentium 4, computer. Convergence is obtained with $M = 11$ entire domain basis functions (aperture field is represented) and with $M = 21$ pulse basis functions (each pole current of the probe is represented).

The computation has been carried out to sample the electric field (without probe) and co-pole voltage in the transverse (x-y) scan

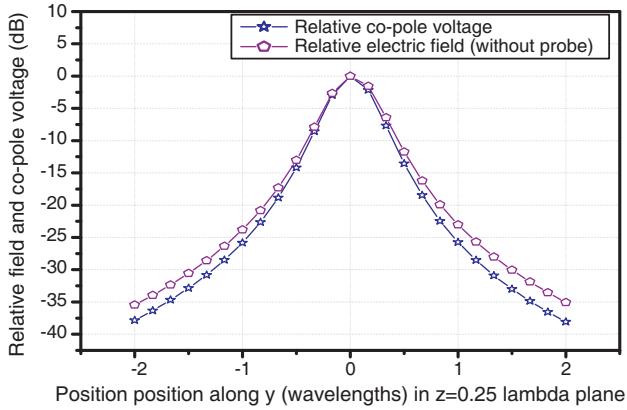

Figure 3. Relative sampled electric field (without probe) and relative sampled co-pole voltage in x-y plane at $x = 0$, $z = 0.25\lambda$, and at 10 GHz.

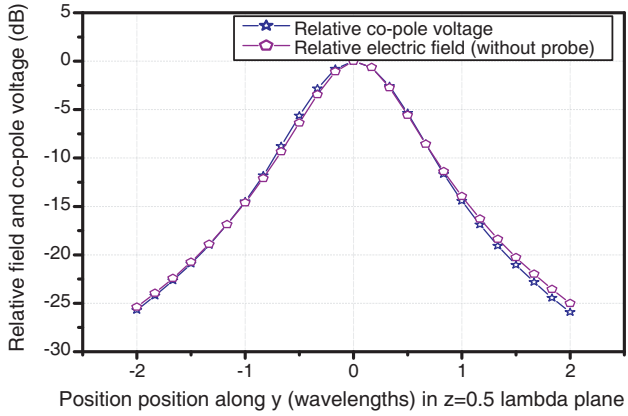

Figure 4. Relative sampled electric field (without probe) and relative sampled co-pole voltage in x-y plane at $x = 0$, $z = 0.5\lambda$, and at 10 GHz.

plane (First case) at 10 GHz to compare the normalized (relative) sampled electric field pattern (without probe) with the normalized (relative) sampled co-pole voltage pattern. Since the normalized values are taken, zero error is enforced at the center of the scan plane. These plots are shown in Figures 2, 3 and 4 in the scan plane at $x = 0$, and $z = 0.15\lambda$, 0.25λ and 0.5λ respectively. The error in the normalized voltage pattern with respect to the normalized electric field (without probe) pattern is estimated. The radiator absolute reflection coefficients in the presence of the near-field measuring probe with each pole length $L = 1.41$ cm and radius $a_w = 0.015$ cm (designed

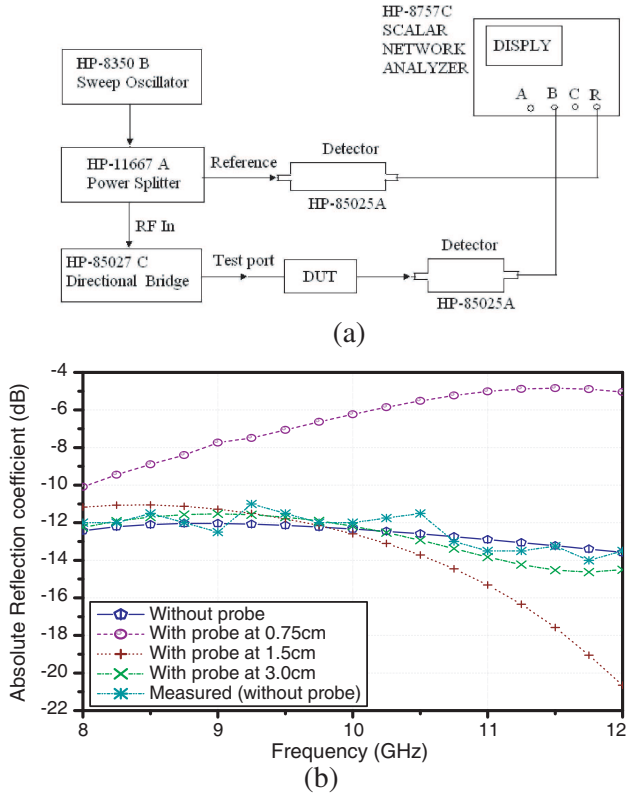

Figure 5. (a) Experimental setup used to measure reflection coefficient. (b) Waveguide radiator reflection coefficient (abs.) in the presence of the crossed-dipole in x-y plane with the length of each pole $L = 1.41$ cm and radius $a_w = 0.015$ cm, over 8 to 12 GHz at $x = 0$, $y = 0$ and $z = 0.75$ cm/1.5 cm/3.0 cm, and in absence of the probe.

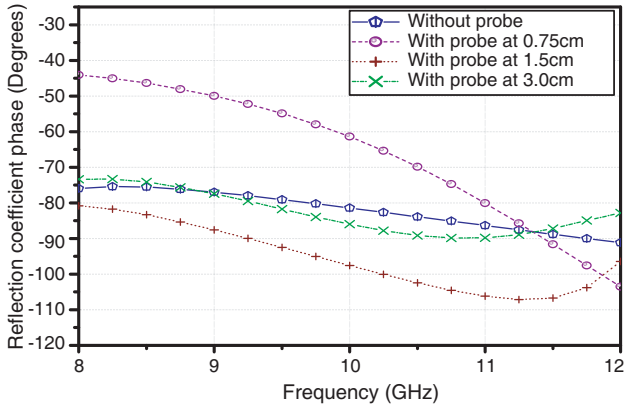

Figure 6. Waveguide radiator reflection coefficient phases in the presence of the crossed-dipole in x-y plane with the length of each pole $L = 1.41\,\text{cm}$ and radius $a_w = 0.015\,\text{cm}$, over 8 to 12 GHz at $x = 0$, $y = 0$ and $z = 0.75\,\text{cm}/1.5\,\text{cm}/3.0\,\text{cm}$, and in absence of the probe.

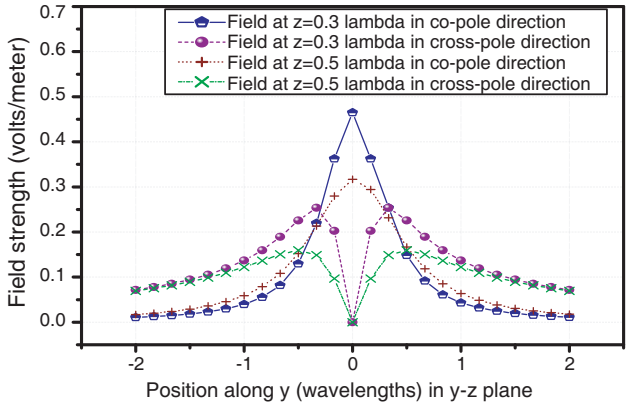

Figure 7. Sampled fields (without probe) in y-z the plane at 10 GHz and at $x = 0$, $z = 0.3\lambda/0.5\lambda$.

at 10 GHz) at $x = 0$, $y = 0$ and $z = 0.75\,\text{cm}/1.5\,\text{cm}/3.0\,\text{cm}$, and in the absence of the probe, over 8 to 12 GHz, are plotted. These results are compared to the measured results and are shown in Figure 5(b). The corresponding reflection coefficient phases are shown in Figure 6. Experiment has been carried out to measure the reflection coefficients of an open-ended waveguide radiator using the scalar network analyzer HP-8757C as shown in the Figure 5(a).

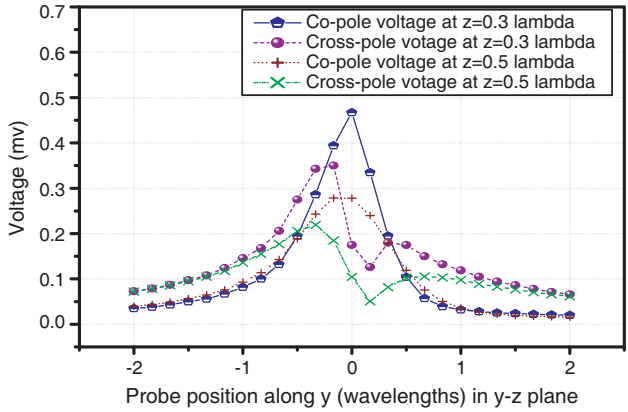

Figure 8. Sampled pole voltages in the y-z plane at 10 GHz and at $x = 0$, $z = 0.3\lambda/0.5\lambda$.

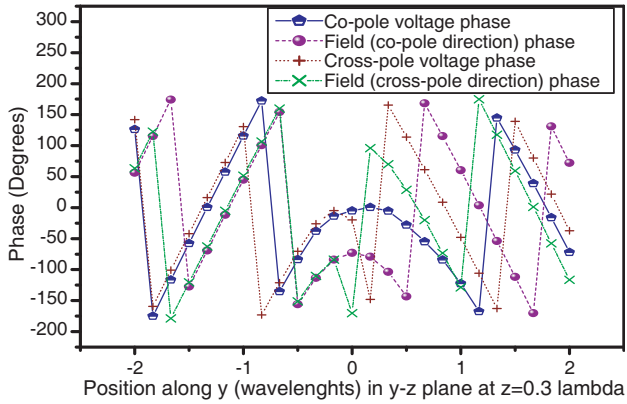

Figure 9. Sampled electric field (without probe) and pole voltage phases in the y-z plane at $x = 0$, $z = 0.3\lambda$, and at 10 GHz.

In the second case, the probe is in the longitudinal (y-z) plane and the cross-pole is parallel to the z-axis. In this case, we cannot compare the electric field pattern (without probe) with the induced cross-pole voltage pattern in the z-direction, since the field in the z-direction is zero at the center of the scan plane and it is non-zero at other positions. Computation has been carried out to determine the sampled fields (without the probe) and sampled pole voltages at $x = 0$ and $z = 0.3\lambda/0.5\lambda$, and at 10 GHz, and these plots are shown in Figures 7 and 8. Also, the sampled electric field (without probe) and pole voltage phases at $x = 0$, and $z = 0.3\lambda/0.5\lambda$, are shown in Figures 9 and 10.

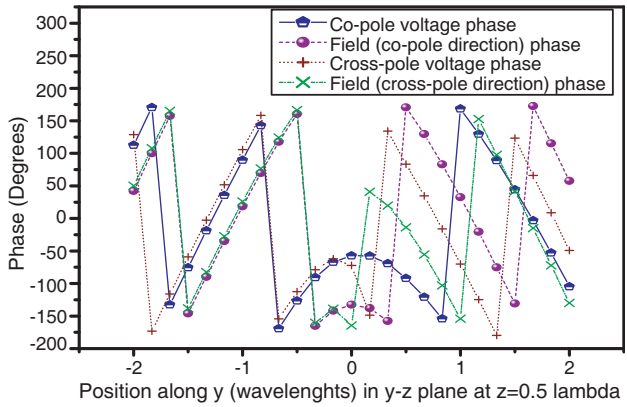

Figure 10. Sampled electric field (without probe) and pole voltage phases in the y-z plane at $x = 0$, $z = 0.5\lambda$, and at 10 GHz.

6. CONCLUSION

The crossed-dipole, which is used as a near-field measuring probe induces error in the near-field, because of multiple reflections between the radiator and probe, and effects of mutual coupling between poles of the probe. In the presence of the near-field measuring probe, the radiator reflection coefficient is changed. When the separation between radiator and the probe is small, the deviation of the reflection coefficient is large with respect to the corresponding values when there is no near-field probe. As the separation increases, the deviation is smaller, and for larger separation, the reflection coefficient values approach the values obtained, when there is no probe in the near-field. The variations of the fields at the near-field are same as the theoretically predicted; this shows the validation of the present formulation. Since the junction of the cross of the probe is taken as the reference and it is not at the center of poles, the maximum co-pole voltage is slightly deviated from the center of the scan plane. Similarly the minimum cross-pole voltage is slightly deviated from the center of the scan plane

REFERENCES

1. Harrington, R. F., *Time-harmonic Electromagnetic Fields*, McGraw-Hill, New York, 1961.
2. Harrington, R. F., *Field Computation by Moment Method*, Roger E. Krieger Publishing Company, USA, 1968.

3. Richmond, J. H., "Digital computer solutions of the rigorous equations for scattering problems," *Proceedings of the IEEE*, Vol. 53, 796–804, 1965.
4. Paramesha, S. and A. Chakrabarty, "Moment method analysis of rectangular waveguide as near-field measuring probe," *MOTL*, Vol. 48, No. 9, 2006.
5. Paramesha, S. and A. Chakrabarty, "Waveguide as a near-field measuring probe of the two-element array radiator," *Progress In Electromagnetics Research B*, Vol. 7, 245–255, 2008.
6. Gupta, S., A. Bhattacharya, and A. Chakrabarty, "Analysis of an open-ended waveguide radiator with dielectric plug," *IEE Proc. Microwave, Antenna and Propagation*, Vol. 144, No. 2, 126–130, 1997.
7. Pisano III, F. A. and C. M. Butler, "Methods for modeling wire antenna loaded with shielded network," *IEEE Trans. on Antennas and Propagation*, Vol. 52, No. 4, 2004.